

Multi-temporal geomorphometric analysis to assess soil erosion under different tillage practices: A methodological case study

Sara Cucchiaro,^{1,2} Laura Carretta,³ Paolo Nasta,⁴ Federico Cazorzi,¹ Roberta Masin,³ Nunzio Romano,^{4,5} Paolo Tarolli²

¹Department of Agricultural, Food, Environmental and Animal Sciences, University of Udine, Udine; ²Department of Land, Environment, Agriculture and Forestry, University of Padova, Legnaro (PD); ³Department of Agronomy, Food, Natural Resources, Animals and Environment, University of Padova, Legnaro (PD); ⁴Department of Agricultural Sciences, AFBE Division, University of Naples Federico II, Portici (NA); ⁵The Interdepartmental Centre for Environmental Research (C.I.R.A.M.), University of Naples Federico II, Portici (NA), Italy

Abstract

Soil erosion is one of the main environmental threats to sustainability and crop productivity in the agricultural sector. In agricultural fields, no-till management is considered a key approach for mitigating soil erosion. The measurement of soil erosion is particularly challenging, especially when surficial morphological changes are relatively small. Conventional experiments are commonly time-consuming and labour-intensive in terms of both field surveys and laboratory methods. On the other hand, the structure from motion (SfM) photogrammetry technique has enhanced the experimental activities by enabling the temporal evolution of soil erosion to be assessed through detailed micro-topography. This work presents a multitemporal quantification of soil erosion, using SfM through uncrewed aerial vehicles (UAV) survey for understanding the evolution of no-till (NT) and conventional tillage (CT) in experimental plots. Considering that morphological

changes at the plot scale had millimetre orders of magnitude, it was necessary to minimise SfM errors (e.g., co-registration and interpolation) in volumetric estimates to reduce noise as much as possible. Therefore, a methodological workflow was developed to analyse and identify the effectiveness of multi-temporal SfM-derived products, e.g., the conventional difference of digital terrain models (DoDs) and the less used differences of meshes (DoMs), for soil volume computations. We validated the erosion volumetric changes calculated from the SfM outputs with the amount of soil directly collected through conventional runoff and sediment measurements in the field. In this way, we recognised the most suitable estimation method. This study presents a novel approach for using DoMs instead of DoDs to describe the micro-topography changes and sediment dynamics accurately. Another key and innovative aspect of this work often overlooked in soil erosion studies, was identifying the contributing sediment surface by delineating the channels potentially routing runoff directly to water collectors. The sediment paths and connected areas inside the plots were identified using a multi-temporal analysis of the sediment connectivity index for achieving the volumetric estimates, using DoMs (e.g., 2213 cm³ for no-till management system - NT and 38155 cm³ for conventional tillage regime - CT during September 2018-June 2020) that showed mild overestimation respect to field measurements results (e.g., 2359 cm³ for NT and 4525 cm³ for CT in the same period). This difference was attributable to other factors (e.g., the soil compaction processes) or variables rather than to photogrammetric or geometric ones. The developed workflow enabled low cost quantification of soil erosion dynamics for assessing the mitigation effects of no-till management that can also be extended in the future to different scales, based on SfM and UAV technologies.

Correspondence: Sara Cucchiaro, Department of Agricultural, Food, Environmental and Animal Sciences, University of Udine, via delle Scienze 206, 33100 Udine, Italy.
E-mail: sara.cucchiaro@uniud.it

Key words: Digital terrain analysis; sediment connectivity; structure from motion photogrammetry; micro-topography; surface runoff.

Acknowledgements: we thank Roberto Degan for his invaluable assistance in collecting runoff water samples and help in field surveys.

Funding: this study was supported by University of Padova research projects BIRD CPDA144499/14 and DOR2079232/20.

See online Appendix for additional materials.

Received for publication: 21 September 2021.
Accepted for publication: 7 December 2021.

©Copyright: the Author(s), 2022
Licensee PAGEPress, Italy
Journal of Agricultural Engineering 2022; LIII:1279
doi:10.4081/jae.2022.1279

This article is distributed under the terms of the Creative Commons Attribution Noncommercial License (by-nc 4.0) which permits any non-commercial use, distribution, and reproduction in any medium, provided the original author(s) and source are credited.

Introduction

Soil erosion induced by water is one of the main environmental threats leading to the degradation of agricultural land worldwide (Morgan, 2009). The soil surface continuously evolves during erosion events. Therefore, erosion processes can cause considerable morphological variations that can profoundly affect agricultural practices depending on the volume of soil removed from the soil surface. Therefore, the accurate measurement of soil erosion rates is becoming a key factor in promoting efficient recovery management types.

Soil erosion in agricultural landscapes occurs primarily due to interrill and rill erosion (Hänsel *et al.*, 2016; Di Stefano *et al.*,

2017). Overland flow triggers the formation of small channels, rills, which can evolve into gullies. Instead, dispersed flow produces diffuse erosion and leaves little trace after an erosion event (in the literature, it is referred to as sheet or interrill erosion). Diffuse erosion is a complex mixture of shallow non-incised concentrated, and dispersed flows and occurs neither in sheets nor between rills (Cândido *et al.*, 2020). In many regions, the diffuse forms of erosion (interrill erosion, tillage erosion, harvest erosion) represent significant contributions to soil sedimentation.

The no-till (NT) management system is considered a key approach for reducing soil erosion in agricultural fields (Schuller *et al.*, 2007). No-till minimises the mechanical soil disturbance and includes managing crop residues, which are left on the field after crop harvesting, maintaining the soil surface partially covered with stubble and straw. A significant reduction of soil erosion and runoff in NT systems compared to tilled soils has been reported by several studies, both under simulated and measured rainfall, even during the transition period from conventional to a no-till system (Carretta *et al.*, 2021).

Measuring soil erosion is quite burdensome and unfeasible for large-scale applications stemming from time-consuming field surveys and financial efforts. The measurement of diffuse and sheet erosion provides a grand challenge because it is difficult to monitor in the field due to its shallow depth and distributed nature, considering the small changes in soil elevation (Pineux *et al.*, 2017).

Several methods have been used to estimate soil erosion with plot-scale modelling (Parsons, 2019). However, in most cases, they are difficult to implement on a wide scale. Traditionally, these frequent measurements are carried out using reference stakes or with profile meters (Pineux *et al.*, 2017) through surveying with terrestrial laser scanner (TLS; Kaiser *et al.*, 2018).

In this framework, cost-effective measurement techniques supported by new-generation technology achieve relevance and interest results with respect to conventional approaches. Among the most widely used new technologies, the structure from motion (SfM) photogrammetry technique paired with multi-view stereo (MVS) algorithms (hereinafter jointly referred to as SfM; Carrivick *et al.*, 2016), is very useful to carry out frequent and detailed topographic surveys (De Marco *et al.*, 2021) for soil erosion monitoring (Eltner *et al.*, 2015; Hänsel *et al.*, 2016; Di Stefano *et al.*, 2019; Cândido *et al.*, 2020). The combination of SfM and widespread uncrewed aerial vehicles (UAVs) offers the opportunity to carry out rapid and cost-effective surveys compared to time-consuming and expensive field measurements based on conventional approaches. Various studies compared the UAV results with those from TLS for soil erosion surveys (Eltner *et al.*, 2015) and demonstrated that the advances in photogrammetric technique enhance data quality and spatial resolution compared to laser scanners and conventional photogrammetry. Indeed, the SfM technique easily adapts to the millimetre scale resolution required to describe diffuse and sheet erosion processes (Balaguer-Puig *et al.*, 2018). Promising results were obtained in field surveys based on the SfM technique to detect changes in soil erosion plots (Di Stefano *et al.*, 2017; Pineux *et al.*, 2017; Balaguer-Puig *et al.*, 2017; Cândido *et al.*, 2020). These authors exploited multi-temporal SfM surveys to obtain high-resolution and detailed digital terrain models (DTMs) by describing the soil erosion evolution. Indeed, DTMs of differences (DoDs) can usually be calculated to detect spatial changes in the soil surface topography over time and quantify the volumes of sediments lost or gained (Mauri *et al.*, 2021).

Since morphological changes at the plot scale are millimetre orders of magnitude, it is necessary to minimise errors in volumetric estimates from topographic surveys to distinguish actual ero-

sion processes from noise due to uncertainties. Systematic error (e.g., the survey accuracy of the equipment and registration errors), the density and distribution of data points used to represent the surface, the missing data due to shadowing effects from vegetation or other obstructions, and interpolation methods to derive DTMs from the SfM data, can contribute to spatially distributed errors in the datasets (Nourbakhshbeidokhti *et al.*, 2019). If some problems inherent to the measurement technique or instrumentation cannot be reduced, the errors of the raw data (*i.e.*, the point clouds) could be analysed. For example, the uncertainty due to the transformation of the point cloud into a continuous elevation surface (e.g., mesh), and the subsequent gridding (*i.e.*, DTMs generation), could be decreased by using the 3D information for volume calculations (*i.e.*, the comparison between multi-temporal meshes). Indeed, the application of the DoDs is a 2.5D environment, where DTMs have an assigned mean elevation at the centre of each pixel, and a topographic data reduction occurs when point cloud data are transformed from 3D to 2.5D (Barnhart and Crosby, 2013). However, this method introduces grid elevation uncertainty or artefacts in three-dimensional environments and overhanging areas. Therefore, considering only the transformation of the point clouds into continuous elevation surfaces (*i.e.*, data interpolation), it could be possible to realise multi-temporal differences of meshes (DoMs) and obtain very accurate soil erosion volumes as it has never been achieved before. Additionally, it is essential to consider the errors and their spatial distribution for each point cloud in assessing the actual topographic changes between different SfM surveys and directly propagate this information on DoMs. These aspects have been poorly analysed in the body of literature.

The study presented in this paper aimed at estimating plot-scale microtopographic changes due to erosive processes, using different multi-temporal UAV-SfM-derived products: the conventional DoDs and the DoMs. We validated the erosion volumetric changes calculated using direct runoff and sediment measurements from the two approaches. This allows us to identify the best estimation method. The workflow was tested in six experimental plots at the Padova University Experimental Farm, three in a conventionally tilled (CT) field and three in a non-tilled field. Multi-temporal SfM surveys were carried out to measure soil erosion under conventional tillage and no-till management through grids and meshes volume information. The SfM point cloud uncertainties were assessed through the generation of precision estimates based on a Monte Carlo approach (James *et al.*, 2017b), operating directly on raw data to distinguish actual erosion processes from spatially variable noise in triangulation (*i.e.*, DoMs) and gridding (*i.e.*, DoDs) outputs. Moreover, since agricultural operations influence the micro-topography that modifies the soil surface roughness, and process dynamics, a sediment connectivity analysis was performed to identify portions of soil surface that were more connected to runoff water collectors and prone to erosion in the experimental plot (Prosdocimi *et al.*, 2017). This innovative aspect often overlooked in soil erosion studies, allowed the identification of the contributing sediment surface to obtain volumetric estimates that were more comparable with field measurements.

The developed workflow can provide helpful information for optimising the monitoring of erosion processes and understanding the sediment dynamics in no-till and conventional tillage systems. Furthermore, these analyses can be extended in the future to different spatial scales with low costs by exploiting SfM and UAV technologies.

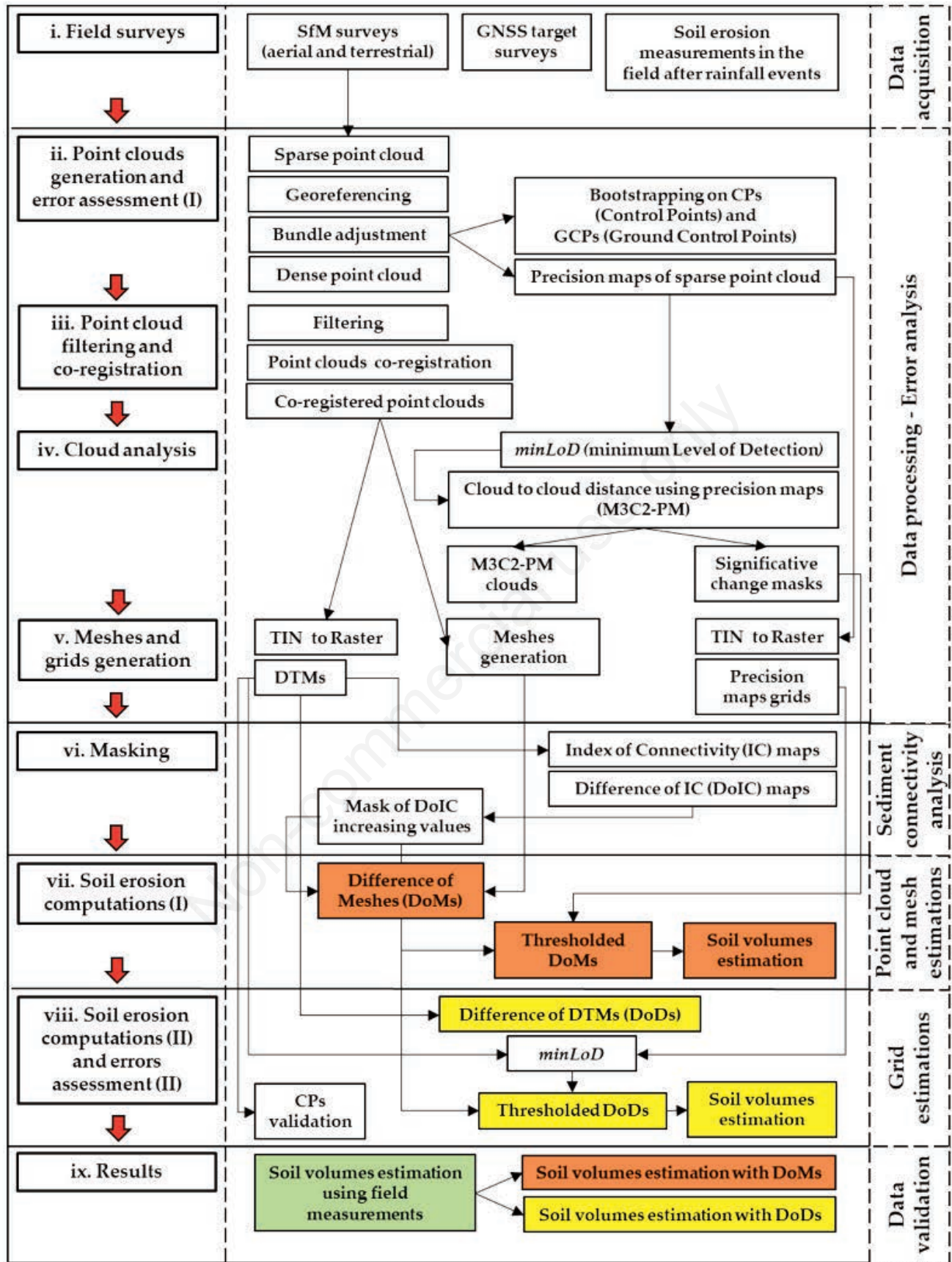


Figure 1. General workflow of the analysis developed in this study (see the text for more details).

Workflow

A workflow (Figure 1) is designed to apply a detailed and standard procedure to multi-temporal SfM surveys and identify soil erosion volumes in the CT and NT experimental plots.

High-resolution topographic survey

Data acquisition

Mission planning is a key aspect, especially to survey micro-topography. A wide range of image acquisition platforms is available, but an integrated approach combining ground-based and aerial images benefits from data acquisition from two different observation directions (*i.e.*, nadir for UAV images and oblique for terrestrial images; Cucchiario *et al.*, 2018). Aerial and terrestrial images (*i.* in Figure 1) should be collected using the same camera with the same focal length to minimize the integration problems in the photogrammetric models and with sufficient overlap between photos to find homologous points within several images (optimal overlap is 80% in flight direction and a flight strip overlap of 60%; Eltner *et al.*, 2016). An additional aspect to consider is the number, location, and distribution of the ground control points (GCPs) and check-points (CPs; *i.* in Figure 1), based on the features of the studied area, extension, and desired resolution. They should be uniformly distributed, not aligned or clustered, and not neglect the margins. GCPs are used in the georeferencing and registration processes to improve the quality of the 3D reconstruction of the terrain surface, while CPs for results validation.

Data processing

The SfM datasets are processed to extract the 3D point clouds and orthomosaics (*ii.* in Figure 1) from the images through photogrammetric software like Agisoft Metashape Pro v 1.6.2 based on SfM and MVS algorithms (James *et al.*, 2017a). The first step in SfM processing workflow is the camera pre-calibration using Agisoft Lens, a starting point for the parameter refinement in the following process, *i.e.*, the SfM phase, where ground-based and UAV photos should be processed together in Metashape to avoid subsequent data fusion problems at the point-cloud level (Cucchiario *et al.*, 2018). In the next step, georeferencing of the 3D sparse point clouds is carried out using the traditional solution of the GCP coordinates (*ii.* in Figure 1). In light of this georeferencing data, the SfM solutions are being improved through a bundle adjustment step algorithm (least-squares network optimisation; Carrivick *et al.*, 2016; *ii.* in Figure 1), through appropriate weighing of tie and control point image observations to enhance a real error characterisation (James *et al.*, 2017a). This is followed by the processing of high-density point clouds and orthomosaics, which involves using an MVS image-matching algorithm. Finally, the georeferenced SfM point clouds are imported into the CloudCompare software (Omnia Version 2.12.2; <http://www.danielgm.net>) to be filtered through different steps (*iii.* in Figure 1): manual filtering, a ‘distance filter procedure’, and the ‘SOR filter tool’. The SOR filter is used to remove outliers by computing the average distance of each point to its neighbours. The manual filter and a ‘distance filter procedure’ helps to delete unwanted objects in the point cloud (*e.g.*, blades of grass, crop residues, and metal partition boards of sub-plots) as illustrated in Cucchiario *et al.* (2020a), differentiating the ground from the other points.

The filtered SfM point clouds must be co-registered (*iii.* in Figure 1) to minimise residual inaccuracies of the georeferencing

process and to guarantee the coherence among multi-temporal surveys, minimising, on stable areas, the distance between corresponding points acquired at a different time (Cucchiario *et al.*, 2020b). The iterative closest point (ICP) automatic algorithm implemented in CloudCompare is used to co-register multi-temporal SfM point clouds and check the manual identification of markers in the images, which could produce inaccurate georeferencing and could lead to an unreal shift or rotation between 3D models. Therefore, the combined use of ICP and GCPs allows a ‘double registration process’ to increase the quality of the point clouds. The ICP should be used on a subset of the point clouds located in stable areas (*e.g.*, metal boards; ditches crossing structures) where no change occurred between the SfM acquisitions, and then the obtained rigid transformation (matrix) should be applied to the whole-original point clouds. The co-registered point clouds were converted in meshes through CloudCompare software (*v.* in Figure 1).

The point clouds are decimated through the geostatistical Topography Point Cloud Analysis Toolkit (ToPCAT). This tool, successfully used in several studies, reduces the point cloud into a set of non-overlapping grid-cells and is manageable by geographic information system (GIS) software, calculating the statistics for the observations in each grid. Next, the decimated point clouds are used to calculate a triangular irregular network (TIN) in Esri ArcGIS software and converted to raster through a natural neighbour interpolator, resulting in one DTM for each SfM survey (*v.* in Figure 1).

Error analysis

Different analyses are carried out at different steps to evaluate the accuracy and precision of the obtained point clouds and DTMs. Firstly, a bootstrapping resampling (1000 times) approach (Marteau *et al.*, 2017) is chosen to estimate the output accuracy and precision of the SfM clouds (*ii.* in Figure 1). One-third of the GCPs are randomly selected as CPs to provide an independent measure of uncertainty for each point (*i.e.*, the residuals or the difference between the real coordinates of this point and the modelled values; Cucchiario *et al.*, 2018). Then, after completing all iterations, during which the bundle adjustment step is reset, the accuracy and precision are obtained for each point when used as GCP or CP. Moreover, following the numerical method proposed in James *et al.* (2017b), the precision maps of SfM surveys are performed to evaluate the spatial variability of the whole point cloud precision (*ii.* in Figure 1), which is influenced by photogrammetric and georeferencing conditions. This method consists of repeated bundle adjustments in Agisoft Metashape through Python script, in which different pseudo-random offsets are applied to the image observations and to the control measurements to simulate observation measurement precision. The Monte Carlo approach enables the tie point error distribution to be quantified for a specific SfM survey and the integration of this information into confidence-bounded change detection (see next Section: *Multi-temporal analysis for soil erosion computations*). Precision estimates for each optimised model parameter are then imported into the ‘sfm_georef’ software (James and Robson, 2012). The software post-processed the Monte Carlo outputs files (*i.e.*, sparse point clouds) to characterise point coordinate precision estimates, variance-covariance, and other metrics from a large number of adjustments, obtaining a precision point cloud for each multi-temporal SfM survey. Then, the vertical standard deviation for each point derived by the precision clouds (σ_z) is used to calculate a TIN in Esri ArcGIS software and converted to raster through a natural neighbour interpolator to realise the precision maps grids of each DTM.

The transformation of the point cloud into a continuous elevation surface (*i.e.*, data interpolation), and the subsequent gridding, introduced several uncertainties or artefacts, especially in the vertical component. Therefore, the accuracy and precision evaluation of the geospatial products are also calculated through a statistical comparison between Z values of CPs (surveyed in the field by GNSS) and the equivalent Z measurements extracted from DTMs (*vii.* in Figure 1). First, following the approach of Höhle and Höhle (2009), the outliers are removed by applying a threshold (*i.e.*, 2 times the root mean square error (RMSE), chosen considering the distribution of errors in the different surveys, keeping an approach that is as precautionary as possible) selected from an initial calculation of the error measures. Then, RMSE, standard deviation (SDE), mean error (ME), and the normalized median absolute deviation (NMAD), a robust estimator for the SDE more resilient to outliers in the dataset (Cucchiario *et al.*, 2020a), are calculated.

Sediment connectivity analysis

Since agricultural operations influence the micro-topography that modifies the soil surface roughness and sediment connectivity, especially at fine spatial scales as highlighted in Tarolli *et al.* (2019), this aspect must be considered in the sediment delivery processes estimations (Di Stefano and Ferro, 2017; Pineux *et al.*, 2017). The concept of connectivity and the geomorphometric indices developed for this aspect are exploited to analyse the sediment dynamic in the experimental plots. Sediment connectivity represents sediment transfer in a system from a source to a sink (*e.g.*, runoff collection system) through sediment detachment and transport per defined unit time. The index of connectivity (IC) proposed in Cavalli *et al.* (2013) allows the identification of the potential sediment paths and the effect of sediment connectivity within each plot. This index primarily analyses the influence of topography on sediment connectivity. It considers the characteristics of the drainage area (upslope component, D_{up}) and the flow path length that a particle must travel to reach the nearest sink or the target of the analysis (downslope component, D_{dn}). The IC is computed as follows (Eq. 1):

$$IC = \log_{10} (D_{up} / D_{dn}) \quad (1)$$

Moreover, the differences of IC (DoIC) are calculated by subtracting the IC map at time 1 from the IC map at time 2 for each plot to investigate the sediment dynamics changes during the time and identify the modification in the connected areas in each subplot for different SfM surveys. Then, DoIC maps for each plot are classified into three classes of connectivity: ‘increase’ (*i.e.*, values of DoIC >0), ‘no change’ (*i.e.*, values of DoIC =0), and ‘decrease’ (*i.e.*, values of DoIC <0) because *i)* each plot could have different patterns of sediment connectivity, which vary in time whether or not consecutive rainstorms occur, and *ii)* not all the soil within the plots could be connected to the outlet. Therefore, the portions of soil that are more connected to the outlet and increased sediment connectivity are reasonably those that will be more prone to erosion once the rainstorm occurs. Consequently, the surface changes maps related to two successive SfM surveys (see next Section: *Multi-temporal analysis for soil erosion computations*) are masked on the ‘Increase’ class of DoIC identified for the corresponding data (*vi.* in Figure 1).

Multi-temporal analysis for soil erosion computations

Using topographic data in the experimental plots, the estimation of soil erosion is realised in different ways: at mesh and grid

level. Therefore, the difference in eroded sediment estimates over time are assessed directly at the raw data level (*i.e.*, mesh; *vii.* in Figure 1) and using the rasterised products (*i.e.*, DTMs; *viii.* in Figure 1). Then, the soil erosion estimates through the topographic survey must be compared (*ix.* in Figure 1) with sediment erosion measurements directly conducted under natural rainfall conditions in the field (*i.* in Figure 1).

Point cloud and mesh estimations

In the first case, the co-registered and filtered point clouds of the different SfM surveys are used as inputs in the multiple model to model cloud comparison (M3C2) tool of CloudCompare (Lague *et al.*, 2013) and integrated with the “precision maps” (M3C2-PM; *iv.* in Figure 1) variant of James *et al.* (2017b). M3C2-PM is particularly suited to point clouds generated by photogrammetric processing and calculated a local normal cloud-to-cloud distance for each selected point in the reference clouds (identified by considering the clouds with greater precision and density of points), incorporating 3-D precision estimates from an associated point cloud as calculated in Section: *Error analysis*. First, precision values (in X, Y, and Z directions) are ascertained directly from the maps for each point pair (i_1 and i_2). Then, based on established error analysis (Lane *et al.*, 2003), the position uncertainty for each pair of points derived from precision estimates is used to determine a confidence interval (or minimum level of detection; *minLoD*; *iv.* in Figure 1) for this distance measurement. The confidence interval for the distance measured in the normal direction, N , is then determined using the components of precision in that direction, σ_{N1} and σ_{N2} , according to Equation 2:

$$\min LoD = t \sqrt{(\sigma_{N1})^2 + (\sigma_{N2})^2} \quad (2)$$

Where t is the Student’s t -score (a value of $t=1.96$ is used for a conservative approach, corresponding to a confidential interval of 0.95, *i.e.*, *minLoD95%*). The output from M3C2-PM thus represents 3-D change between SfM point clouds along with the normal local directions, assessing whether that change exceeds the local LoD95% values (changes above *minLoD* were considered ‘significant’), derived from the 3-D spatially variable photogrammetric and georeferencing precision. The M3C2-PM information in terms of significant or non-significant change associated at each point cloud is used to realize shapefiles (*i.e.*, polygons) that defined the valuable areas to be considered in soil erosion volumetric calculations (*vii.* in Figure 1). Therefore, the meshes realized from co-registered and filtered point clouds (see Section: *Data processing*; *v.* in Figure 1) are cut out by considering only the areas with significant changes (*iv.* in Figure 1) between two different surveys. In addition, the areas where the sediment connectivity did not increase over time (*i.e.*, negative values of DoIC, identified in Section: *Sediment connectivity analysis*; *vi.* in Figure 1) between two different surveys are further removed on the mesh patches with significant changes. The meshes restricted in terms of significant changes and positive DoIC values are imported into the JRC 3D Reconstructor Gexcel software, where the ‘Cut and fill’ tool is used to realise the difference between two meshes (difference of meshes; DoMs) and calculate erosion and deposition soil volumes in consecutive surveys (*vii.* in Figure 1). Given two meshes representing the same object (*e.g.*, the same subplot) at different times, the cut volume is the volume that the object lost between time 1 and 2 (*i.e.*, erosion process), whereas the fill volume is the volume that the object gained between the two SfM surveys (*i.e.*, deposition process). The tool considers two surfaces, S_1

and S_2 , and a plane P , and assuming that the projections of S_1 and S_2 on P share a support C in common, a third surface, S_{min} , can be defined. Since each point in C is the projection on P of (at least) one point of S_1 and one of S_2 , the closest point to P is defined as belonging to S_{min} . Let V_1 be the integral of S_1 on C , V_2 the integral of S_2 on C , and V_{min} the integral of S_{min} on C . Then the soil erosion volume V_{cut} is given by $V_1 - V_{min}$ and the soil deposition volume V_{fill} is $V_2 - V_{min}$ (Reconstructor Gexcel, 2021). This allows the estimation of soil erosion and deposition volumes in time directly at mesh level (vii. in Figure 1) without the need to go through the rasterization process..

Grids estimations

In the second case, the difference between a DTM (obtained as described in Section: *Data processing*) and the previous one (*i.e.*, DTM of differences; DoDs) enabled the calculation of the total volumes of erosion, deposition, and net change during the time. DTM uncertainty and error propagation (viii. in Figure 1) are considered in the analysis to obtain reliable DoDs and to discriminate between the actual difference in surface elevation and background noise. The significance of DoD difference is the thresholded by applying a *minLoD* as in Section: *Point cloud and mesh estimations*. Changes above *minLoD* are considered real, but when the changes were below the *minLoD*, these are classified as uncertain and not used in the final computation (Lane et al., 2003). The uncertainty level of each DTM is assessed through the precision maps (see Sections: *Error analysis* and *Point cloud and mesh estimations*; James et al., 2017b). The precision maps grids (realised as described in Section: *Error analysis*) are used as error surface estimates for each DTM and propagated into the DoDs as spatially variable vertical uncertainties. A *minLoD* of significant elevation change is calculated for each DoDs cell, according to Equation 3:

$$\text{minLoD} = t \sqrt{(\sigma_{z1})^2 + (\sigma_{z2})^2} \quad (3)$$

Where σ_{z1} and σ_{z2} are the vertical precision estimates for each cell in the two DTMs and t is the Student's t -distribution value defined by a specific confidence level (this study 95%, giving $t = 1.96$). Thus, changes smaller than the *minLoD* can be disregarded, and the GCD software for ArcGIS is used to generate the *minLoD*-thresholded DoD maps. Thresholded DoDs provide a difference in elevation for each grid cell; thus, knowing the size of each cell, the elevation changes were transformed to volumes (viii. in Figure 1). Also, the thresholded DoDs and raw DoDs (*i.e.*, DoD where the DTM uncertainty and error propagation were not applied) are restricted in terms of positive DoIc area (vi. in Figure

1) to identify soil erosion volumes connected to sediment collection tanks (viii. in Figure 1).

A case study at the Experimental Farm of the University of Padova in the Po Valley, north-eastern Italy

The study was conducted during the period September 2018–June 2020 at the Experimental Farm of the University of Padova in the Po Valley, north-eastern Italy (45°20'43"N, 11°56'58"E, altitude 6 m a.s.l.; Figure 2A). The local climate is sub-humid with a mean annual temperature of 13.6°C (value calculated as the average of the monthly mean temperatures from January 1994 to December 2020). Annual rainfall was 853 mm with 89 rainy days in 2018, 866 mm with 89 rainy days in 2019, and 702 mm with 74 rainy days in 2020. Six sub-plots (each 2.5×5 m; Figure 2A and B) were established in spring 2017 (Carretta et al., 2021). Three plots are located in a field managed under a conventional tillage regime (CT plot), and the other three are in a field under no-till management (NT plot). The fields measure 0.7 ha, and the slope was 2.7% for both NT and CT fields. The two fields faced each other and were separated by a ditch (Figure 2B). Each sub-plot is bounded on three sides by metal boards inserted 15 cm below-ground, 15 cm protruding above the soil surface to prevent any splash effect or runoff flowing either out of or into adjacent sub-plots. Each sub-plot was initially equipped with a runoff water collection system with a 55 L tank. However, in July 2018, the runoff collectors of the CT plots were replaced with 100 L tanks because in a few cases overflowing runoff volumes were collected after intense rainfall events (Figure 2C).

Harrowing was performed on the CT field in April 2018. Maize was sown at the end of April 2018, and it was harvested in September 2018. The CT field was ploughed to a 25–30 cm depth in October 2018, followed by harrowing. At the end of October 2018, both fields were sown with wheat, harvested at the end of June 2019. In October 2019, the CT field was ploughed to a 25–30 cm depth and harrowed, and wheat was sown in both fields at the end of October 2019. The wheat harvesting was carried out at the end of June 2020 (Figure 2A). In NT, crop residues have always been left on the field after the harvesting of each crop.

Data acquisition

Three photogrammetric surveys were conducted on NT and CT plots, as summarised in Table 1. Previous crop residues were temporarily removed from the NT plots to allow the execution of the surveys and then placed again onto the plots. Aerial and terres-

Table 1. Detail and main characteristics of structure from motion surveys.

Date		September 2018	November 2019	June 2020
Area (m ²)		75	75	75
Field conditions		8 days after maize harvesting	Seven days after wheat sowing	Three days after wheat harvesting
Number of targets		30 [10]	30 [10]	30 [10]
GNSS survey	Positional accuracy (X, Y, Z) (m)	<0.05	0.03–0.04	0.03–0.04
	Reference system	RDN2008/UTM zone 32N (EPSG: 6707)	RDN2008/UTM zone 32N (EPSG: 6707)	RDN2008/UTM zone 32N (EPSG: 6707)
SfM survey	Number of images	308	337	333
	Flight height (m)	8	8	8
	Ground sample distance (m)	0.002	0.002	0.002

GNSS, global navigation satellite system; SfM, structure from motion.

trial images (*i.* in Figure 1) were collected with a Sony Alpha 5000 compact digital camera (20 Mpixels, focal length 20 mm, sensor size 23.2×15.4 mm). For the aerial survey, the camera was mounted on a professional 8-rotors UAV (Neutech Airvision NT-4C). A manual flight mode was used with the camera's time-lapse function that allowed to capture images (nadir and oblique) at 2 s intervals, sufficient to guarantee the overlap in sequential photographs. Indeed, test flights indicated that flying at 1 m/s ensured a sufficiently large overlap (80% in flight direction and a flight strip overlap of 60%) and a high image footprint (Table 1). For the ground-based surveys, the photographs were taken by maintaining an adequate average distance from the object; a mean baseline (0.5 m) between adjacent camera positions avoided large jumps in scale and minimised the interval between the images to reduce the effects of change in lighting conditions. Before acquiring the images, GCP and CP were placed in the study area (Figure 1B),

avoiding the formation of clusters or preferential lines and maintaining similar inter-distances to obtain a homogeneous distribution. The SfM targets comprised square orange cloth with a black rhombus in the middle, an old compact disk (standard diameter of 120 mm) placed in the centre (*i.e.*, CD-ROMs; see Figure 2A). The targets were located around the study area, while old compact disks were used as markers and placed inside the plot areas to occupy less space. The CD-ROMs were chosen as targets because they are small, the central hole is suitable for inserting the global navigation satellite system (GNSS) pole with high precision, and they were easily detectable in the photos. Therefore, CD-ROMs represented a suitable and low-cost solution for measuring GCPs and CPs. The spatial coordinates of targets were measured with a GeoMax Zenith 40 GNSS in Relative Stop&Go post-processed mode (*i.* in Figure 1) to have a more accurate solution and control on raw GNSS data.

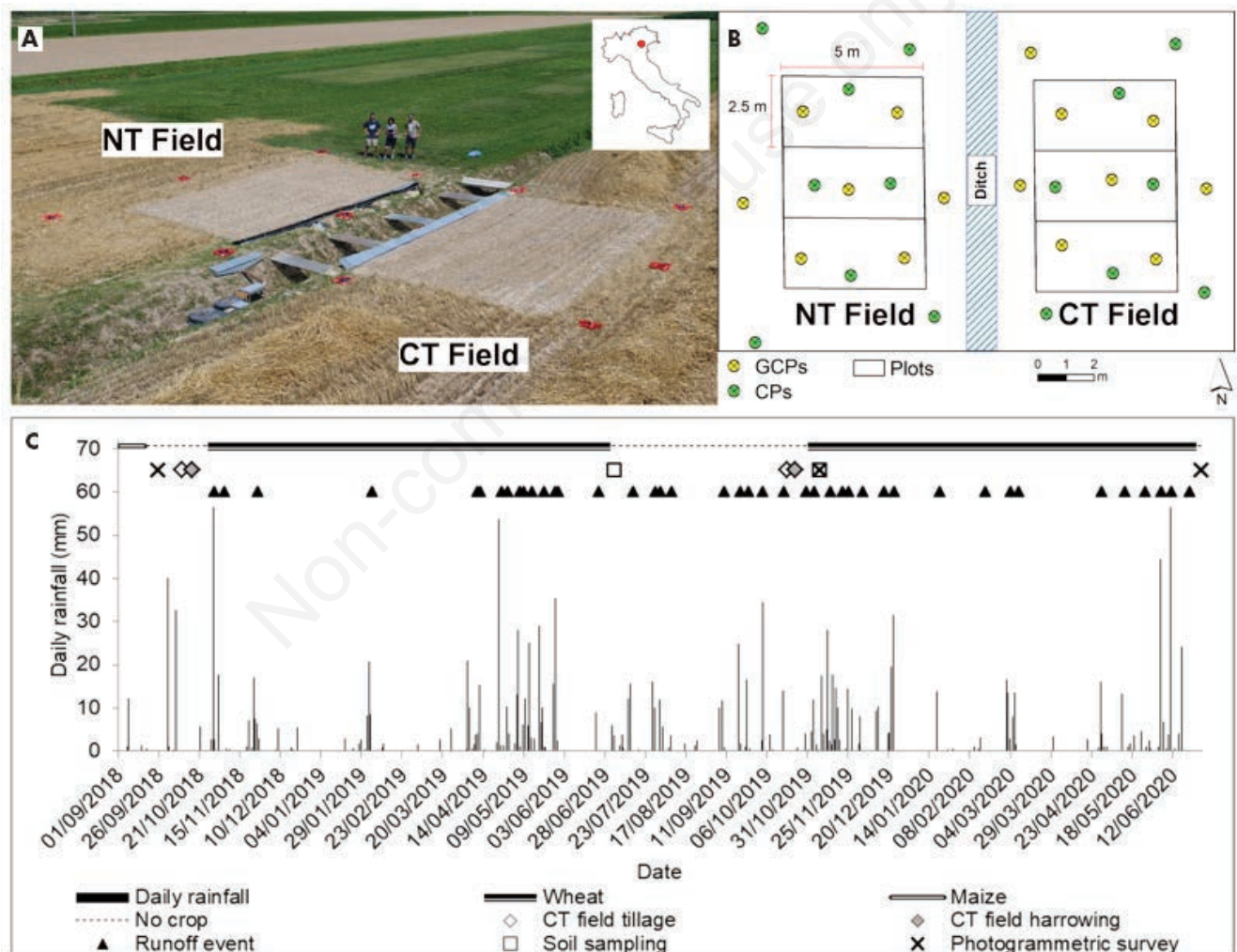


Figure 2. The study area. A) Panoramic overview of the whole agricultural landscape at the Padova University Experimental Farm where the experimental plots are located. Three plots are in a field managed under a conventional tillage regime (CT plot), and the other three in a field managed using no-tillage practice (NT plot); B) Schematic drawing of the experimental sub-plots and the locations of control points (CPs) and ground control points (GCPs) during structure from motion surveys; C) Daily rainfall monitored from September 2018 to June 2020. Runoff events, soil samplings, photogrammetric surveys, tillage operations, and crops cultivated in the NT and CT fields are indicated at the top.

Data processing, error analysis, and sediment connectivity

The SfM surveys were processed as described in Section: *Data processing* to obtain georeferenced, filtered, and co-registered. For the co-registration process, the point cloud of November 2019 was chosen as a reference because it presented a good precision and accuracy in terms of CPs (see next Section: *Structure from motion data processing and error analysis* and Table 2). The co-registered point clouds were converted in meshes (*v.* in Figure 1) and decimated through ToPCAT (see Section: *Data processing*) allowing the selection of a grid cell of 0.02 m, considering the minimum elevation within each grid cell. The same cell size of 0.02 m was used to realise the precision maps grids of each DTM, following the workflow in Section: *Data processing*.

The IC was applied to DTMs of each sub-plot using the stand-alone application SedInConnect based on Python scripting with bindings for processing geographical datasets (Crema and Cavalli, 2018). The runoff collection system of each sub-plot was used as a sink in the IC computations to identify areas potentially connected to each collection tank and therefore contributing to the volumes measured in the field.

Data validation using field measurements

The soil erosion estimates through the topographic survey were compared (*ix.* in Figure 1) with sediment erosion measurements directly conducted under natural rainfall conditions in the field (*i.* in Figure 1). The Regional Agency for Environmental Protection (ARPAV) meteorological station on the experimental farm, 30 m far from the plots, with a rain gauge recording every 5 min, was used to measure rainfall events (Figure 2C). The technique adopted for measuring soil erosion, already described in Carretta *et al.* (2021), is rather simple and cost-effective. The total runoff water volume collected in the tanks was measured for each runoff-generating rainfall event, and three 0.5-L water samples were collected in aluminium bottles from each sub-plot (Figure 2A and B). The samples were then transferred into plastic containers and placed in a dryer at 60°C for 48 h. When all the water had evaporated, the samples were weighed to obtain the sediment yield for erosive events. Sediment concentration was multiplied by the runoff volume to determine the sediment yield from each sub-plot at each runoff event.

To determine the oven-dry soil bulk density (BD), in November 2017, one month after soybean harvesting, in July 2019 after wheat harvesting, and in November 2019, two weeks after the CT field's seedbed preparation, undisturbed soil samples were collected from both the NT and CT fields next to the runoff plots. At each sampling date, three sampling locations were selected on the

CT and six on the NT field. Among the six sampling locations on the NT field, three were on the no-track (NT no-track) and three on the track position (NT track), the latter being the portion of soil affected by tractor wheels' passage (Figure 2A). The soil samples were collected at 15-20 cm depth using cylindrical steel cores (height, 7.0 cm; internal diameter, 7.2 cm) and then placed in a labelled plastic bag, sealed, and transported to the laboratory. The bulk density measured in November 2017 was 1.66 ± 0.067 , 1.74 ± 0.069 , and 1.55 ± 0.083 g/cm³ for NT track, NT no-track, and CT, respectively. The bulk density measured in July 2019 was 1.59 ± 0.050 , 1.58 ± 0.099 , and 1.47 ± 0.023 g/cm³ for NT track, NT no-track, and CT, respectively. The bulk density measured in November 2019 was 1.57 ± 0.053 , 1.60 ± 0.069 , and 1.43 ± 0.069 g/cm³ for NT track, NT no-track, and CT, respectively. To test for significant differences ($P < 0.05$) of soil bulk density between sampling dates for each sampling location and between sampling locations for each sampling date, a one-way ANOVA followed by Tukey post-hoc test was performed using RStudio Version 1.4.1106 (RStudio Team 2021). The bulk density values were not significantly different between the different sampling dates for NT track, NT no-track, and CT samples; moreover, no significant differences in bulk density were observed between the NT samples taken at the track and no-track position for each sampling date. The mean bulk density of NT and CT soils was calculated by averaging the bulk density values of all the sampling dates without discriminating between track and no-track positions for the NT soil. The mean bulk density is 1.62 and 1.48 g/cm³ for NT and CT soil, respectively.

The soil mass from each sub-plot at each runoff occurrence was summed over all events that happened within the monitoring period interspersed with the different SfM surveys and converted into volume data using the mean bulk density information.

Results and discussion

Structure from motion data processing and error analysis

By processing SfM, high-quality, dense point cloud (12,801,448, 11,002,321, and 5,947,619 points, with a mean density of 170,685, 146,697, and 79,301 points/m², respectively over September 2018, November 2019, and June 2020 surveys) meshes, and DTMs were obtained. These datasets were adequate to identify micro-topographic features of experimental plots. Table 2 summarises the point quality analysis of the GCPs and CPs in terms of

Table 2. Errors assessed for structure from motion point clouds and their derived digital terrain models.

	Point clouds							DTMs				
	Accuracy CPs			RMSE _{3D} *	Precision CPs		Georeferencing GCPs RMSE _{3D} *	MAE	SDE	RMSE ^o	NMAD [#]	
	(m)	(m)	(m)		(m)	(m)						(m)
September 2018	0.0132	0.0117	0.0590	0.0706	0.0115	0.0104	0.0381	0.0500	0.0436	0.0647	0.0739	0.0716
November 2019	0.0160	0.0098	0.0065	0.0228	0.0093	0.0070	0.0051	0.0192	0.0329	0.0393	0.0380	0.0315
June 2020	0.0159	0.0099	0.0065	0.0239	0.0094	0.0071	0.0050	0.0191	0.0353	0.0341	0.0346	0.0311

CP, control points; GCP, ground control points; DTMs, digital terrain models; MAE, mean of the residuals; SDE, standard deviation of the residuals; RMSE, root mean square error; NMAD, normalized median absolute deviation. Note: For structure from motion surveys, the bootstrapping technique applied in Agisoft Metashape after all the iterations provides MAE as an indication of the accuracy of the georeferencing process and the point cloud when GCP and CP residuals are used, respectively, while SDE yields an indication of the precision. *RMSE_{3D} (3D root mean square error) of GCPs and CPs computed along the x, y, and z directions; ^othe outliers were removed by applying a threshold (2 times the RMSE) selected from an initial calculation of the RMSE measures (Höhle and Höhle, 2009); [#]NMAD: proportional to the median of the absolute differences between errors and the median error (Höhle and Höhle, 2009).

precision, accuracy, and georeferencing error for each SfM survey carried out. In addition, the bootstrap resampling technique (see Section: *Error analysis*) enabled detailed SfM errors to be evaluated, which were all in the order of magnitude of centimetres, and thus suitable for investigating soil erosion processes at the plot scale as stated in different works (Eltner *et al.*, 2015; Balaguer-Puig *et al.*, 2017; Kaiser *et al.*, 2018).

The precision maps calculated in Agisoft Metashape for each SfM cloud showed a spatial variation of mean point precision of 22 mm, 6 mm, and 9 mm for September 2018, November 2019, and June 2020 surveys, respectively. The spatial variation of precision maps was related to the image overlap and the UAV flights due to the manual mode navigation, which required operator care to achieve the necessary coverage of the area of the plots. In addition, other factors that influence the precision of SfM models were the presence of vegetation and soil roughness, as highlighted in different studies as Eltner *et al.* (2015), James *et al.* (2017b), and Cândido *et al.* (2020). The precision of the obtained SfM results highlighted that the acquisition of images from two different observation directions (*i.e.*, oblique and nadir) and platforms (*i.e.*, UAV and ground-based) led to an optimal camera network geometry (*i.e.*, great image overlap and high angle of convergence), and fewer deformation errors or area distortions. Several pieces of research confirmed that the addition of oblique photographs in a UAV survey considerably strengthens the network geometry (Eltner *et al.*, 2016). This also allowed reducing the errors in estimated camera parameters and the likelihood of detectable systematic DTM error, such as the ‘doming effect’. The possibility to exploit different acquisition platforms is certainly one of the strengths of the SfM surveys. In the case of the experimental plots discussed in this paper, the nadir perspective allowed a more effective survey of the points compared to techniques of terrestrial acquisition and more classic as the TLS.

Table 2 shows the DTM errors for each survey, underlining the high quality of the final outputs obtained from SfM data by comparing CPs measured in the field. These statistics also highlighted how the interpolation process (*i.e.*, gridding) slightly increased the errors in DTM data compared to the errors at the point cloud level for all statistical values analysed. This is the well-known problem of the gridding process that induced a loss of resolution and increased errors compared to the original data (Chaplot *et al.*, 2006; Heritage *et al.*, 2009). As in Li *et al.* (2004), further analysis could be done to improve the DTM errors estimations and confirm the shown results. Similar results were presented in Nourbakhshbeidokhti *et al.* (2019), where errors were significantly smaller in point clouds before triangulation than in DTM as converting a LiDAR (laser imaging detection and ranging) point cloud to grids increases the error by interpolation. However, the quality of the DTMs obtained was certainly high (centimetre-level), considering the values in Table 2, which demonstrated how the SfM process proved effective in generating very high-resolution topographic (HRT) data. Also, Balaguer-Puig *et al.* (2017) stated that at the plot scale, erosive processes could lead to very small surface variations, and high precision DTMs were needed to account for differences measured in millimetres. The wide range of calculated metrics allowed a more robust error estimation, especially after the outlier removal, making the statistics more reliable (Höhle and Höhle, 2009). Moreover, using metrics such as NDAM further reinforced the data obtained from other statistics as being very similar. Several authors have stated the importance of using robust accuracy assessment methodology and metrics, preferably not influenced by outliers or by a skew in the distribution of the errors (Wang *et al.*, 2015).

The ICP errors obtained in CloudCompare software for the co-registration processes of the different SfM survey show RMSE of 0.045 and 0.031 m in stable areas for the September 2018–November 2019 and November 2019–June 2020 point cloud pairing, respectively. The choice to start the ICP process from the overlapping stable areas and then extend the co-registration process to the whole area certainly improved the quality of the multi-temporal survey alignments, as demonstrated in several studies (Cucchiari *et al.*, 2020b). The co-registration procedure enabled noise reduction and better identification of the actual changes in multi-temporal surveys.

Sediment connectivity analysis

Figure 3 depicts the IC maps highlighting how the sediment connectivity changed over time due to rainfall events and agricultural practices. The multi-temporal sediment connectivity analysis proved useful to identify soil zones potentially connected to runoff collectors and more prone to water erosion and zones not directly connected to the plot outlet. Indeed, the potential connected areas (*i.e.*, yellow boundaries in Figure 3A, C, and E) are only 13%, 54%, and 40% of the whole surface represented by the experimental plots respectively in September 2018, November 2019, and June 2020. The remaining sediment volumes showed a tendency not to be virtually mobilisable and, therefore, were not accounted for in the estimation of eroded soil volumes. The areas contributing to sediment production further decrease when analysing the IC values since only the portions of the plots in the Medium-High and High IC classes (*i.e.*, the caption in Figure 3) may be considered the most likely to produce erosive processes, *i.e.*, only 10% (0.93 m²), 4% (1.31 m²) and 3% (0.76 m²) of the entire potentially connected area (*i.e.*, yellow boundaries in Figure 3A, C, and E) respectively for September 2018, November 2019, and June 2020 surveys. This point also proved valid in work presented by Prosdocimi *et al.* (2017), where the consideration of the only high values of IC for masking the elevation differences maps in multi-temporal SfM surveys yielded results of the same order of magnitude between erosion measurements obtained by topographic and traditional methods. Furthermore, sediment connectivity analysis emphasized the higher IC values of the CT than NT conditions: 18% (0.60 m²), 4% (1 m²) and 3% (0.47 m²) for CT with respect to 5% (0.33 m²), 2% (0.35 m²) and 2% (0.29 m²) for NT correspondingly for September 2018, November 2019, and June 2020 surveys.

In this work, a step further than the study presented by Prosdocimi *et al.* (2017) was realised because the multi-temporal component of connectivity (*i.e.*, DoIC maps in Figure 3B, D, and F) was considered, and then the only areas with IC increments (*i.e.*, positive DoIC values) between two successive surveys were used to identify potentially mobilisable sediment. Also, sediment connectivity analysis with DoIC highlighted the different sediment dynamics of agricultural lands under NT and CT conditions. Indeed, the CT plots presented higher IC values in the Medium-High and High classes than NT considering the entire potentially connected surface: 18%, 4%, and 3% (CT) with respect to 5%, 2%, and 2% (NT) correspondingly for September 2018, November 2019, and June 2020 surveys. This feature persists over time, also analysing the ‘increase DoIC’ values (Figure 3B, D, and F) for the same areas: 2%, 5%, and 2% (CT) with respect to 1%, 3%, and 1% (NT) correspondingly for September 2018, November 2019, and June 2020 surveys. This phenomenon can be explained by analysing the different micro-topography resulting from current agricultural treatments. As stated by Tarolli *et al.* (2019): NT areas were characterized by rougher surfaces, with more pronounced

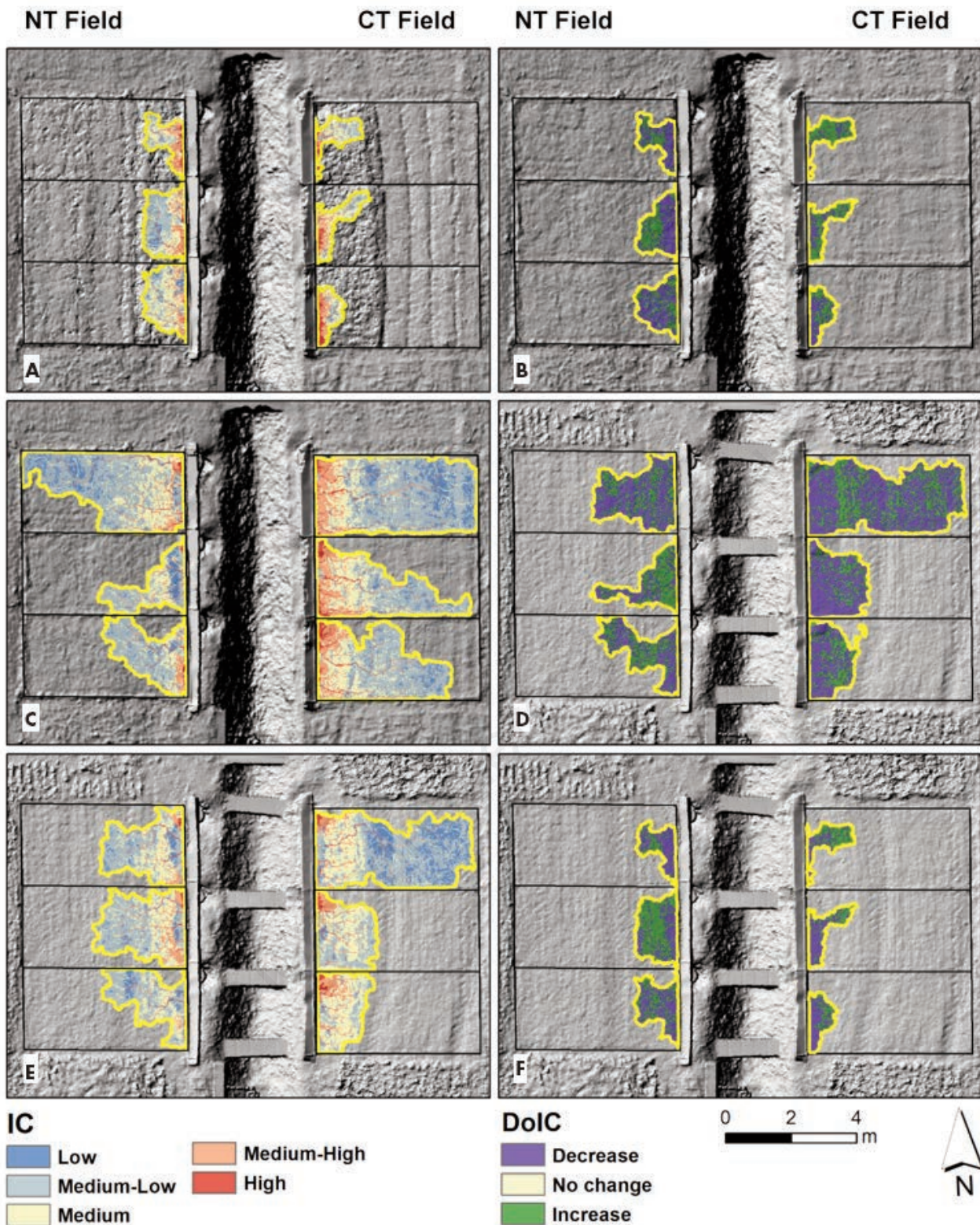


Figure 3. Index of connectivity (IC) and differences of IC (DoIC) maps for experimental plots realised through digital terrain models (DTMs). In the background, the shaded relief map of DTMs used for the analysis. Based on the Natural Breaks classification methods, the IC values have been classified into five classes (low, medium-low, medium, medium-high, and high). A) the IC map of September 2018; B) the DoIC map of September 2018-November 2019; C) the IC map of November 2019; D) the DoIC map of November 2019-June 2020; E) the IC map of June 2020; F) the DoIC map of September 2018-June 2020.

concavities and convexities (due to no-tillage conditions and preferential tractor paths during the harvesting process), while CT surfaces were smoother than NT less than one month after seedbed preparation. Generally, tilled soil presents rougher surfaces soon after the seedbed preparation, representing the best conditions for the crop seedling emergence. The micro-depression or furrows generated by the tillage can store water and erode sediment during rainfall events, but the accumulation of sediment in surface depressions or furrows results in smoothing the soil surface over time. Instead, after several years of no-tillage, it is expected that the surface morphology and soil aggregated will be stable and consolidated. Therefore, a terrain with the NT condition was likely to reduce overland flow (quantity) and velocity (energy) and thus sediment connectivity that may significantly change the soil delivery at the outlet (Pineux *et al.*, 2017). These results confirm the importance of micro-topography in sediment connectivity and, consequently, in estimating eroded materials.

Soil erosion computations and data validation

Figure 4 provides a visual quantification of soil erosion over time by exploiting raw data (*i.e.*, point clouds and meshes in Figure 4A, B, and C) and the rasterised products (*i.e.*, DoDs; Figure 4D, E, and F). The M3C2-PM clouds show the geomorphic change in experimental plots with a high level of detail. The M3C2-PM mean distance was -0.033 m with 0.048 m standard deviation, -0.020 m mean with 0.025 m standard deviation, -0.060 m mean with 0.050 m standard deviation, respectively for September 2018–November 2019, November 2019–June 2020, and September 2018–June 2020 clouds (Figure 4A.1, B.1, and C.1). Also, at the corresponding grid level (*i.e.*, DoDs; Figure 4D, E, and F), the topographic changes were evident for NT and CT plots. The significant changes in the maps at point cloud level (Figure 4A.2, B.2, and C.2) and the corresponding raster data (*i.e.*, DoDs; Figure 4D, E and F) highlighted how the topographic difference was subject to an important degree of uncertainty and noise. In fact, the rasterised precision maps allowed the thresholding of raw DoDs (Figure 4D, E, and F) and the identification of actual morphological changes as in the M3C2-PM point clouds. Several researchers stress the importance of thresholding and uncertainty estimation in the soil erosion process, such as Cândido *et al.* (2020), who affirmed the usefulness of raster precision maps for removing insignificant topographical changes. As in this study, Balaguer-Puig *et al.* (2018) stated that setting an error threshold was fundamental to quantify small-magnitude soil erosion at the plot scale, while Balaguer-Puig *et al.*

(2017) highlighted how the choice of different threshold values in the DoDs could lead to volume differences as large as 60% when compared to the direct volumetric difference. Also, Eltner *et al.* (2015) underlined that minimal changes in minLoD had a significant influence on laminar changes; thus, HRT data accuracy was more relevant for estimating diffuse erosion and levelling processes than rill erosion. The effectiveness of using an uncertainty threshold to identify reliable erosional processes is confirmed by the volumetric data calculated from the DoMs and DoDs compared to those measured in the field, which acts as ground truth (Table 3). Table 3 demonstrated how the thresholded maps enabled the elimination of some residual phenomena of unrealistic deposition due to possible systematic errors and filtering of crop residues (particularly in NT plots; Figure 4D). As happened in the September 2018–November 2019 survey, raw DoD and DoM showed a positive net volume difference, which is impossible in a closed system with only sediment loss. The thresholded DoDs and DoMs displayed lower volumetric estimates than raw data and were closer to those measured with field sediment collection systems, removing some of the uncertainty of all topographic surveys.

The results in Table 3 confirmed the ongoing erosional processes illustrated in Figure 4 and their low magnitude, which is difficult to identify without very accurate surveys. Indeed, the volumes estimated by processing SfM data show net negative differences, indicating widespread erosion phenomena throughout the monitoring period (*i.e.*, September 2018–June 2020). During the period November 2019–June 2020, volumetric estimates obtained from topographic surveys were very high for all quantification methods (*i.e.*, DoDs and DoMs) compared to collected sediment measurements. This could be due to the presence of wheat crop residues that were difficult to remove without removing soil information in the filtering process in the June 2020 SfM survey. An overestimation of topographic volumes was generally found (except for NT volumes measured by DoMs during September 2018–November 2019) when compared with direct measurements (Table 3). Previous laboratory studies reported similar soil loss overestimation, usually attributed to soil settling within the simulation box and bulk density changes due to raindrops compaction (Gessesse *et al.*, 2010). Hänsel *et al.* (2016) offered crucial evidence of how the validation of SfM photogrammetry that determined soil loss estimations with rainfall simulation measurements were solely possible due to the consideration of soil compaction processes in agricultural landscapes. The authors applied a height correction to the DoD cell values to compensate for supposed soil

Table 3. Comparison between sediment erosion measurements directly conducted under natural rainfall conditions in the field and soil erosion estimates through structure from motion survey obtained from difference of digital terrain models and differences of meshes areas in Figure 4.

Survey	Sediment erosion collection in the field Soil volumes* (cm ³)		Raw DoDs Net volume difference ^o (cm ³)		SfM surveys Thresholded DoDs Net volume difference ^o (cm ³)		Raw DoMs Net volume difference ^o (cm ³)		Thresholded DoMs Net volume difference ^o (cm ³)	
	NT	CT	NT	CT	NT	CT	NT	CT	NT	CT
September 2018–November 2019	1225.134	3080.544	1181.689	-39,230.905	-2623.809	-33,456.633	213.886	-12,598.792	-905.273	-9682.214
November 2019–June 2020	1134.752	1445.150	-29,027.242	-51,660.248	-28,598.717	-48,225.507	-24,234.134	-40,033.805	-23,526.995	-35,656.994
September 2018–June 2020	2359.886	4525.693	-11,236.501	-79,464.741	-9280.055	-79,464.741	-2722.149	-38,288.126	-2213.762	-38,155.128

SfM, structure from motion; DoDs, differences of digital terrain models; DoMs, differences of meshes; NT, no-till; CT, conventional tillage. Note: The \pm uncertainty of the thresholded DoDs volumes was estimated considering a minLoD . *Raw DoDs' are DoD where the digital terrain models uncertainty and error propagation were not applied, while 'Raw DoMs' means the difference of meshes were not cut out considering the areas with significant changes between two different surveys. ^oThe soil mass from experimental plots was converted into volume data using the mean bulk density information; ⁿnet volume changes were the difference between deposition and erosion volumes.

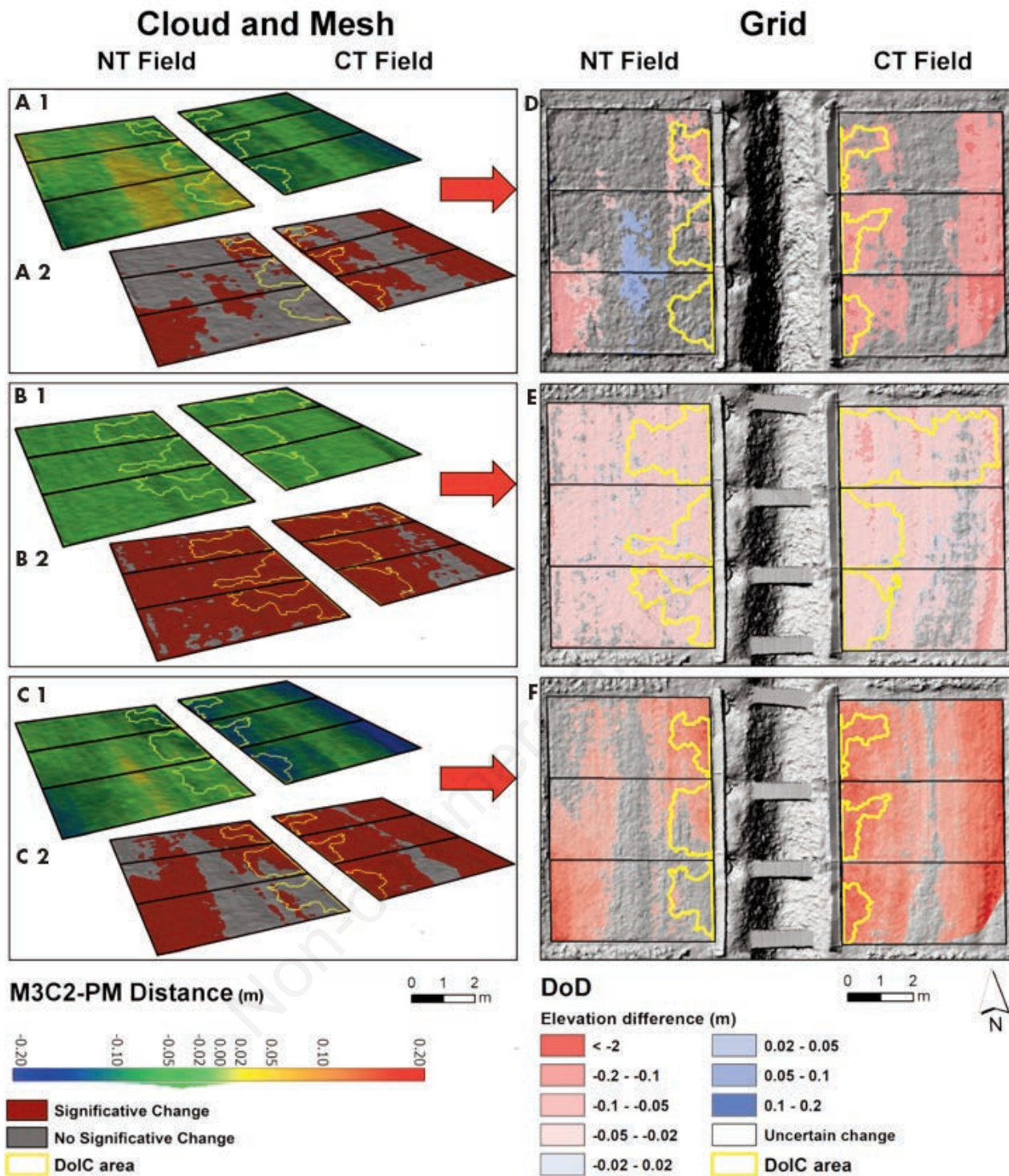


Figure 4. Geomorphic change detection using multitemporal clouds and grids data for the experimental plots where the differences of index of connectivity (DoIC) areas used for the volume computations of the soil erosion are shown. (A.1) Multiple model to model cloud comparison-precision maps (M3C2-PM) point cloud distances and (A.2) their significant change maps used to mask the meshes between September 2018 and November 2019 point clouds; (B.1) M3C2-PM point cloud distances and (B.2) their significant change maps between November 2019 and June 2020 point clouds; (C.1) M3C2-PM point cloud distances and (C.2) their significant change maps between September 2018 and June 2020 point clouds; (D) the difference of digital terrain model (DoD) of September 2018-November 2019 and the respective DoIC areas; (E) the DoD of November 2019-June 2020 and the respective DoIC areas; (F) the DoD of September 2018-June 2020 and the respective DoIC areas.

compaction. Balaguer-Puig *et al.* (2018) also reported an overestimation of 13% in accumulated soil loss obtained from SfM-based DoDs compared with actual sediments collected in the field. The authors of the study highlighted how other factors or variables than photogrammetric or geometric ones, as some edaphic issues (*e.g.*, soil settling or bulk density variations), were involved in runoff generation, such as surface roughness or sediment connectivity.

Moreover, Kaiser *et al.* (2018) quantified the influence of non-erosive soil surface processes on sediment loss estimations and volume calculations to critically examine the potential misinterpretations of high-resolution topography data in soil erosion studies. Kaiser *et al.* (2018) verified the hypothesis of the influence of soil physical properties on topographic data. Therefore, soil loss overestimation in Table 3 could be attributed to non-erosive soil surface processes that can lead to significant errors in sediment yield estimation.

The most important thing arising from Table 3 was that thresholded DoMs estimations were closer to the reality of the processes that occurred in the field. Indeed, the thresholded DoMs obtained only through the triangulation of point cloud and M3C2-PM information provided erosion volumes more similar to reference data (*i.e.*, traditional runoff and sediment measures) than DoDs. In particular, the thresholded DoMs show lower volume estimations which denoted a decrease in noise and errors mainly related to the rasterization process. Identifying significant changes by working directly on the point clouds without triangulation or gridding through the M3C2-PM algorithm certainly helped in detailed discrimination between noise and real morphological changes. Similar outcomes were presented by Nourbakhshbeidokhti *et al.* (2019) that stated how the estimation of topographic changes solely based on point comparison (*i.e.*, Cloud to Cloud and M3C2) were more reliable than those that interpolate surfaces (*i.e.*, Cloud to Mesh and DoD). At the point cloud level, it is challenging to make volumetric calculations, and it is necessary to interpolate the data. However, this work demonstrates how more accurate results can be obtained using cloud error information and DoMs rather than the traditional DoDs. A mesh surface can better reconstruct the course of the micro-topography and thus recreate a more detailed terrain morphology in its complexity than a raster product.

Moreover, Heritage *et al.* (2009) highlighted how the interpolation errors increase with local topographic variability. Therefore, the use of DoMs with a high level of detail could be beneficial to describe the processes in place more accurately, especially when it was required to detect micro-topography. Indeed, DoMs could help identify erosive phenomena through topographic techniques reaching accuracies of the same order of magnitude as the elevation changes. However, this methodology has been poorly used in the literature and would merit further analysis, perhaps by doing tests on determining morphological changes with different features and contexts where the reference volumes are known and extremely accurate.

In addition, the outcomes in Table 3 shed light on the differences between erosion phenomena in plots managed with no-till and conventional tillage systems. As already revealed by the multi-temporal analysis of IC within plots (see Section: *Sediment connectivity analysis*), sediment was potentially more mobilisable in the tillage zone. This phenomenon was also confirmed by sediment volumes measured directly in the field and through topographic techniques. Indeed, the erosive processes in tillage plots were more significant than in those managed with non-tilled throughout the SfM monitoring period (Table 3). A similar result for these experimental plots was presented by Carretta *et al.* (2021), where NT practices coincided with reductions of over 50% in runoff volumes

and 50% to 95% in sediment losses with significant on-site benefits in terms of both sustainable soil management and surface water quality. Furthermore, as mentioned in Section: *Sediment connectivity analysis* in NT plots, micro-depressions can readily intercept and trap sediments, which significantly affect the influence of sediment output, highlighting the importance of a rougher surface. These observations are also supported by Tarolli *et al.* (2019) and Wang *et al.* (2017b) and underlined how in a tilled field, surface morphology and soil hydrological properties were subjected to considerable variations over time due to tillage operations and field management. For this reason, detailed and frequent monitoring of soil morphology, using remote sensing techniques and digital terrain analysis, were required to provide a more solid basis from which to draw conclusions.

Conclusions

This work demonstrated how topographic techniques such as SfM through UAV surveys help to understand the sediment dynamics of no-till and conventional tillage in experimental plots over time. However, these results were possible only through a careful analysis of SfM outputs and a detailed workflow that minimises errors such as co-registration and interpolation to distinguish real erosion processes from noise due to uncertainties. The error information was fundamental to threshold different multi-temporal SfM-derived products: the traditional DoDs and the less used DoMs. The validation of the erosion volumetric changes calculated from the SfM outputs with the amount of soil directly collected through traditional runoff and sediment measures in the field showed a slight overestimation of the results, but it was attributable to other factors (*e.g.*, the soil compaction processes) or variables other than photogrammetric or geometric ones. However, the most significant aspect was that the thresholded DoMs obtained only through the triangulation of point cloud and M3C2-PM information provided erosion volumes closer to reference data than DoDs, denoting a decrease in noise and errors mainly related to the rasterization process. Consequently, this work established how the use of DoMs instead of the traditional DoDs could accurately describe the micro-topography and ongoing processes, especially when the magnitude of the elevation changes is low.

Another key aspect that led to achieving volumetric estimates using DoMs comparable to field measurements results was the analysis of multi-temporal sediment connectivity identifying exclusively the areas potentially connected to runoff water collectors. This aspect is often overlooked, and it is erroneously assumed that all the soil within the plots could be connected to the outlet. However, this research demonstrates how, in the monitoring of erosion processes, the sediment connectivity must be considered to obtain an accurate evaluation of the phenomena.

Combining these tools in a specific and detailed workflow allowed us to obtain satisfactory volumetric estimates able to describe in detail how the diffuse erosion processes in tillage plots were greater than in non-tilled. Therefore, the information obtained from the monitoring through multi-temporal UAV-SfM surveys, in addition to the quantification of sediment loss, for later use in models, also could represent detailed spatial and temporal dimensions of the soil erosion dynamics, which is of great importance in understanding the mechanisms of the soil erosion in conventional tillage and no-till system. Furthermore, a constant UAV-SfM monitoring, which can be extended to a larger scale in the future, can provide useful and detailed feedback that can influence

decisions concerning the mitigation of erosion processes, such as choosing the best agricultural management practices to focus on.

References

- Balaguer-Puig M., Marqués-Mateu Á., Lerma J.L., Ibáñez-Asensio S. 2018. Quantifying small-magnitude soil erosion: Geomorphic change detection at plot scale. *L. Degrad. Dev.* 29:825-34.
- Balaguer-Puig M., Marqués-Mateu Á., Lerma J.L., Ibáñez-Asensio S. 2017. Estimation of small-scale soil erosion in laboratory experiments with structure from motion photogrammetry. *Geomorphology*. 295:285-96.
- Barnhart T.B., Crosby B.T. 2013. Comparing two methods of surface change detection on an evolving thermokarst using high-temporal-frequency terrestrial laser scanning, Selawik River, Alaska. *Remote Sens.* 5:281337.
- Cândido B.M., Quinton J.N., James M.R., Silva M.L.N., de Carvalho T.S., de Lima W., Beniaich A., Eltner A. 2020. High-resolution monitoring of diffuse (sheet or interrill) erosion using structure-from-motion. *Geoderma*. 375:114477.
- Carretta L., Tarolli P., Cardinali A., Nasta P., Romano N., Masin R. 2021. Evaluation of runoff and soil erosion under conventional tillage and no-till management: a case study in northeast Italy. *Catena* 197:104972.
- Carrivick J.L., Smith M.W., Quincey D.J. 2016. *Structure from motion in the geosciences*. John Wiley & Sons, Ltd, Chichester, UK.
- Cavalli M., Trevisani S., Comiti F., Marchi L. 2013. Geomorphometric assessment of spatial sediment connectivity in small Alpine catchments. *Geomorphology*. 188:31-41.
- Chaplot V., Darboux F., Bourennane H., Leguëdois S., Silvera N., Phachomphon K. 2006. Accuracy of interpolation techniques for the derivation of digital elevation models in relation to landform types and data density. *Geomorphology* 77:126-41.
- Crema S., Cavalli M. 2018. SedInConnect: a stand-alone, free and open source tool for the assessment of sediment connectivity. *Comput. Geosci.* 111:39-45.
- Cucchiario S., Cavalli M., Vericat D., Crema S., Llana M., Beinat A., Marchi L., Cazorzi F. 2018. Monitoring topographic changes through 4D-structure-from-motion photogrammetry: application to a debris-flow channel. *Environ. Earth Sci.* 77.
- Cucchiario S., Fallu D.J., Zhang H., Walsh K., Van Oost K., Brown A.G., Tarolli P. 2020a. Multiplatform-SfM and TLS data fusion for monitoring agricultural terraces in complex topographic and landcover conditions. *Remote Sens.* 12:1946.
- Cucchiario S., Maset E., Cavalli M., Crema S., Marchi L., Beinat A., Cazorzi F. 2020b. How does co-registration affect geomorphic change estimates in multi-temporal surveys? *GIScience Remote Sens.* 57:611-32.
- De Marco J., Maset E., Cucchiario S., Beinat A., Cazorzi F. 2021. Assessing repeatability and reproducibility of structure from motion photogrammetry for 3D terrain mapping of riverbeds. *Remote Sens.* 13:2572.
- Di Stefano C., Ferro V. 2017. Testing sediment connectivity at the experimental SPA2 Basin, Sicily (Italy). *L. Degrad. Dev.* 28:1992-2000.
- Di Stefano C., Ferro V., Palmeri V., Pampalone V. 2017. Measuring rill erosion using structure from motion: A plot experiment. *Catena* 156:383-92.
- Di Stefano C., Palmeri V., Pampalone V. 2019. An automatic approach for rill network extraction to measure rill erosion by terrestrial and low-cost unmanned aerial vehicle photogrammetry. *Hydrol. Process.* 33:1883-95.
- Eltner A., Baumgart P., Maas H.-G., Faust D. 2015. Multi-temporal UAV data for automatic measurement of rill and interrill erosion on loess soil. *Earth Surf. Process. Landforms* 40:741-55.
- Eltner A., Kaiser A., Castillo C., Rock G., Neugirg F., Abellán A. 2016. Image-based surface reconstruction in geomorphometry-merits, limits and developments. *Earth Surf. Dyn.* 4:359-89.
- Gessesse G.D., Fuchs H., Mansberger R., Klik A., Rieke-Zapp D.H. 2010. Assessment of erosion, deposition and rill development on irregular soil surfaces using close range digital photogrammetry. *Photogramm. Rec.* 25:299-318.
- Hänsel P., Schindewolf M., Eltner A., Kaiser A., Schmidt J. 2016. Feasibility of high-resolution soil erosion measurements by means of rainfall simulations and SfM photogrammetry. *Hydrology* 3:1-16.
- Heritage G.L., Milan D.J., Large A.R.G., Fuller I.C. 2009. Influence of survey strategy and interpolation model on DEM quality. *Geomorphology* 112:334-44.
- Höhle J., Höhle M. 2009. Accuracy assessment of digital elevation models by means of robust statistical methods. *ISPRS J. Photogramm. Remote Sens.* 64:398-406.
- James M.R., Robson S. 2012. Straightforward reconstruction of 3D surfaces and topography with a camera: Accuracy and geoscience application. *J. Geophys. Res. Earth Surf.* 117:1-17.
- James M.R., Robson S., D'Oleire-Oltmanns S., Niethammer U. 2017a. Optimising UAV topographic surveys processed with structure-from-motion: Ground control quality, quantity and bundle adjustment. *Geomorphology* 280:51-66.
- James M.R., Robson S., Smith M.W. 2017b. 3-D uncertainty-based topographic change detection with structure-from-motion photogrammetry: precision maps for ground control and directly georeferenced surveys. *Earth Surf. Process. Landforms* 42:1769-88.
- Kaiser A., Erhardt A., Eltner A. 2018. Addressing uncertainties in interpreting soil surface changes by multitemporal high-resolution topography data across scales. *L. Degrad. Dev.* 29:2264-77.
- Lague D., Brodu N., Leroux J. 2013. Accurate 3D comparison of complex topography with terrestrial laser scanner: application to the Rangitikei canyon (N-Z). *ISPRS J. Photogramm. Remote Sens.* 82:10-26.
- Lane S.N., Westaway R.M., Hicks D.M. 2003. Estimation of erosion and deposition volumes in a large, gravel-bed, braided river using synoptic remote sensing. *Earth Surf. Process. Landforms* 28:249-71.
- Li Z., Zhu C., Gold C. 2004. *Digital terrain modeling, distributed hydrologic modeling using GIS*. CRC Press, Dordrecht.
- Marteau B., Vericat D., Gibbins C., Batalla R.J., Green D.R. 2017. Application of Structure-from-Motion photogrammetry to river restoration. *Earth Surf. Process. Landforms* 42:503-15.
- Mauri L., Straffellini E., Cucchiario S., Tarolli P. 2021. UAV-SfM 4D mapping of landslides activated in a steep terraced agricultural area. *J. Agric. Eng.* 52:1130.
- Morgan R.P.C. 2009. *Soil erosion and conservation*. John Wiley & Sons, New York, NY, USA.
- Nourbakhshbeidokhti S., Kinoshita A.M., Chin A., Florsheim J.L. 2019. A workflow to estimate topographic and volumetric changes and errors in channel sedimentation after disturbance. *Remote Sens.* 11:rs11050586.
- Parsons A.J. 2019. How reliable are our methods for estimating soil erosion by water? *Sci. Total Environ.* 676:215-21.

- Pineux N., Lisein J., Swerts G., Bielders C.L., Lejeune P., Colinet G., Degré A. 2017. Can DEM time series produced by UAV be used to quantify diffuse erosion in an agricultural watershed? *Geomorphology* 280:122-36.
- Prosdocimi M., Burguet M., Di Prima S., Sofia G., Terol E., Rodrigo Comino J., Cerdà A., Tarolli P. 2017. Rainfall simulation and structure-from-motion photogrammetry for the analysis of soil water erosion in Mediterranean vineyards. *Sci. Total Environ.* 574:204-15.
- Reconstructor Gexcel, 2021. Online Help Reconstructor 4. Available from: <https://help.gexcel.it/reconstructor/v4/CutFillCalculation.html>. Accessed: 1 September 2021.
- Schuller P., Walling D.E., Sepúlveda A., Castillo A., Pino I. 2007. Changes in soil erosion associated with the shift from conventional tillage to a no-tillage system, documented using 137Cs measurements. *Soil Tillage Res.* 94:183-92.
- Tarolli P., Cavalli M., Masin R., 2019. High-resolution morphologic characterization of conservation agriculture. *Catena* 172:846-56.
- Wang B., Shi W., Liu E. 2015. Robust methods for assessing the accuracy of linear interpolated DEM. *Int. J. Appl. Earth Obs. Geoinf.* 34:198-206.
- Wang L., Dalabay N., Lu P., Wu F. 2017. Effects of tillage practices and slope on runoff and erosion of soil from the Loess Plateau, China, subjected to simulated rainfall. *Soil Tillage Res.* 166:147-56.

Non-commercial use only